Journal of Energy Chemistry 26 (2017) 359–367

Contents lists available at ScienceDirect

Journal of Energy Chemistry

journal homepage: www.elsevier.com/locate/jechem

http://www.journals.elsevier.com/journal-of-energy-chemistry/

A new kinetic model for direct CO_2 hydrogenation to higher hydrocarbons on a precipitated iron catalyst: Effect of catalyst particle size

Ali Nakhaei Pour*, Mohammad Reza Housaindokht

Department of Chemistry, Faculty of Science, Ferdowsi University of Mashhad, P. O. Box: 9177948974, Mashhad, Iran

ARTICLE INFO

Article history:
Received 10 September 2016
Revised 2 December 2016
Accepted 5 December 2016
Available online 14 January 2017

Keywords:
Fischer–Tropsch synthesis
Carbon dioxide hydrogenation
Iron-based catalyst
Kinetic parameters

ABSTRACT

The kinetic of the direct CO_2 hydrogenation to higher hydrocarbons via Fischer–Tropsch synthesis (FTS) and reverse water-gas shift reaction (RWGS) mechanisms over a series of precipitated Fe/Cu/K catalysts with various particle sizes was studied in a well mixed, continuous spinning basket reactor. The iron catalysts promoted with copper and potassium were prepared via precipitation technique in various alcohol/water mixtures to achieve a series of catalyst particle sizes between 38 and 14 nm. A new kinetic model for direct CO_2 hydrogenation was developed with combination of kinetic model for FTS reaction and RWGS equilibrium condition. For estimate of structure sensitivity of indirect CO_2 hydrogenation to higher hydrocarbons, the kinetic parameters of developed model are evaluated for a series of iron catalysts with various particle sizes. For kinetic study a wide range of syngas conversions have been obtained by varying experimental conditions. The results show that the new developed model fits favorably with experimental data. The values of activation energies for indirect CO_2 hydrogenation reaction are fall within the narrow range of 23–16 kJ/mol.

1. Introduction

Increased utilization of CO_2 as a starting material is highly desirable because it is an inexpensive, and nontoxic starting material [1–3]. Carbon dioxide can be chemically converted to fuels or chemical feedstock. However, in order to make a significant contribution to reducing CO_2 emissions, its utilization should focus primarily on the conversion to fuels since the market for chemicals is lower than that for fuels [4,5]. There are many routes are possible for production of synthetic fuels from CO_2 like as Fischer–Tropsch synthesis (FTS) (the established industrial process for converting syngas to liquid fuels). It should also be noted that fuels produced via FTS process are specifically attractive because of their unlimited compatibility with conventional fuels in any proportion [6–8]. However, there is an obvious lack of published techno-economic feasibility studies in this area, which could potentially support this argument. Although, Dimitriou et al. reported that the production costs range from £15.8–29.6 per liter of liquid fuels, for indirect CO_2 hydrogenation [9].

From the thermodynamic and kinetic point of view, CO_2 is an inert molecule and must be made reactive by supplying energy externally [1,10]. A practical solution to solve this problem is the conversion of carbon dioxide to more active molecules such as carbon monoxide, in the indirect CO_2 hydrogenation to higher hydrocarbons [11–13]. In second step, produced carbon monoxide can be converted to heavy hydrocarbons via FTS route. Thus, the conversion of CO_2 to fuels via FTS mechanism has been postulated to be a two-stage reaction mechanism, with initial conversion of CO_2 to CO via reverse water-gas shift (RWGS) reaction, followed by chain growth as observed in FTS reaction [14–18]. Cobalt and iron catalysts have been applied to industrial-scale FTS process. Iron FTS catalysts are active in both water-gas shift (WGS) and reverse water-gas shift (RWGS) reactions [19]. In principle, iron-based catalysts would be ideal candidates used in the FTS routes of CO_2-containing syngas.

The kinetic description of the indirect CO_2 hydrogenation reaction is extremely important for the industrial practice, being a prerequisite for the scale-up, optimization, and simulation. The reaction mechanism for CO_2 hydrogenation to higher hydrocarbons is complex with a large number of reactions and species involved [6,7,10,15,20,21]. For this reason, despite the extensive studies that have been conducted to describe the kinetics of FTS and WGS reactions [22–27], there are very few reports in this area

* Corresponding author.
E-mail addresses: a.nakhaei@um.ac.ir, nakhaeipoura@yahoo.com (A. Nakhaei Pour).

http://dx.doi.org/10.1016/j.jechem.2016.12.006

consist [28,29]. Riedel et al. developed a non-Langmuir–Hinshelwood Hougen–Watson (LHHW) kinetic model using integration and regression features of ASPEN PLUS software for CO_2 hydrogenation on a potassium promoted iron catalyst [14]. Willauer et al. used the kinetic model developed by Riedel et al. for comparison of the results obtained from CO_2 hydrogenation to higher hydrocarbons using a Mn and K-promoted iron catalyst in fixed bed reactor and continuously stirred tank (CSTR) reactor [30]. They found that the maximum C_2–C_{5+} yield obtained in the fixed-bed experiments is 49% higher than those obtained by CSTR at lower gas hourly space velocity [30].

The particle size effect on the FTS rate has been the subject of much investigation as well [18,31–34]. The influence of support type and cobalt cluster size (i.e., with average diameters falling within the range of 8–40 nm) on the kinetics of FTS was investigated by kinetic model by Ma et al. [35]. The CO_2 hydrogenation to higher hydrocarbons is followed by FTS reaction and must be a structure sensitive reaction, which is changed by catalyst particle size.

In this work, a new kinetic model for direct CO_2 hydrogenation to higher hydrocarbons was developed with combination of LHHW kinetic model for FTS reaction that was developed in our previous work [36] and RWGS equilibrium conditions. For evaluation of structure sensitivity of indirect CO_2 hydrogenation to higher hydrocarbons, the kinetics parameters of developed model are evaluated for a series of iron catalysts with various particle sizes. Thus, a series of iron catalysts were prepared by precipitation process in various alcohol/water mixtures to achieve a range of catalyst particle sizes.

2. Kinetic model development

2.1. Kinetic model

The direct synthesis of hydrocarbons from CO_2 and H_2 is accepted as a two-step process. In the first step, CO_2 is reduced to carbon monoxide and water according to the reverse water-gas shift reaction (RWGS) within the overall stoichiometry as below:

$$CO_2 \rightleftharpoons + H_2 \; CO + H_2O \tag{1}$$

For evaluation of rate of the RWGS at different temperatures, the temperature dependency of the thermodynamic equilibrium constant on the water-gas shift (WGS) reaction, K_p, the following relation was used [37]:

$$\log K_p = \log\left(\frac{P_{CO_2}P_{H_2}}{P_{H_2O}P_{CO}}\right) = \frac{2073}{T} - 2.029 \tag{2}$$

In this equation, P_j is the partial pressure of species j. Also, the WGS reaction approaches to equilibrium, described by a parameter q, which is considered as second parameter for evaluation of portion of RWGS at many reaction conditions [38,39]:

$$q = \frac{1}{K_p}\left(\frac{P_{CO_2}P_{H_2}}{P_{H_2O}P_{CO}}\right) \tag{3}$$

The value of q ranges from 0 to 1 as WGS reactions approach equilibrium under FTS condition based on reaction conditions and catalyst compositions. The q parameter is higher than one in most cases for CO_2 hydrogenation, which is passes from RWGS reaction. Thus, the q parameter is not a useful parameter for the direct synthesis of hydrocarbons from CO_2 hydrogenation. It is better to use the reverse value of q, which is defined as r ($r = 1/q$) for CO_2 hydrogenation. In low temperature FTS reaction condition, the WGS reaction is far from thermodynamic equilibrium and the equilibrium constant for WGS reaction can be shown as below [6,40–42]:

$$k_p = \frac{P_{CO_2}P_{H_2}}{P_{H_2O}P_{CO}} \tag{4}$$

Where k_p is lower than K_p in thermodynamic equilibrium condition. In the second step of the direct synthesis of hydrocarbons from CO_2 hydrogenation process, produced carbon monoxide can then further react with hydrogen, according to the overall FTS reaction, which is producing higher hydrocarbons. In addition, carbon monoxide in the presence of water can also be converted back into carbon dioxide and hydrogen following the WGS reaction pathway.

The FTS reaction rate for iron catalysts commonly increases with H_2 partial pressure and decreases with water partial pressure. Many kinetic models are developed for FTS reaction on iron catalysts. In our previous works [36], we developed a useful kinetic model based on enolic mechanism for FTS reaction as following equation:

$$r_{FTS} = \frac{k_{FTS}P_{CO}P_{H_2}}{P_{CO} + bP_{H_2O}} \tag{5}$$

Which k_{FTS} is FTS reaction rate constant, r_{FTS} is hydrocarbon production rate, b is a parameter that is equal to K_3/K_1 ratio, and K_1 and K_3, are adsorption constants for surface adsorption of CO and H_2O molecules, respectively. In addition, P_i is partial pressure of ith component into the reactor. Eq. (5) can be rearrangement as below:

$$r_{FTS} = \frac{k_{FTS}P_{H_2}}{1 + b\frac{P_{H_2O}}{P_{CO}}} \tag{6}$$

If the partial pressure of CO (P_{CO}) is changed by the partial pressure of CO_2 using Eq. (4), the new kinetic reaction for CO_2 hydrogenation (CDH) is obtained based on following equation.

$$r_{CDH} = \frac{k_{FTS}P_{H_2}}{1 + bk_p\frac{P^2_{H_2O}}{P_{CO_2}P_{H_2}}} \tag{7}$$

The reaction rate expression that is given in Eq. (7) can be linearized by rearrangement for simplifying of the data evaluation, as below:

$$\frac{P_{H_2}}{r_{CDH}} = \frac{1}{k_{FTS}} + \frac{a}{k_{FTS}}\frac{P^2_{H_2O}}{P_{CO_2}P_{H_2}} \tag{8}$$

Where $a = bk_p$. Hence a plot of $\frac{P_{H_2}}{r_{CDH}}$ versus $\frac{P^2_{H_2O}}{P_{CO_2}P_{H_2}}$ should give a straight line with intercept of $1/k_{FTS}$ and slope of (a/k_{FTS}). The k_p can be calculated from experimentally partial pressures of the ith component using Eq. (4) for each reaction condition and the partial pressure of the ith component can be calculated using the following formula:

$$P_i = \frac{m_i}{\sum_i^{N_C} m_i}P_T \quad (i = 1, \ldots, N_C) \tag{9}$$

2.2. Parameters estimation in the kinetic model

The rate of hydrocarbon production was fitted into the linearized kinetic model (Eq. (8)), in order to study the effects of the catalyst particle size on the kinetic parameters of the CO_2 hydrogenation to higher hydrocarbons in the present work. The recognition of the kinetic models and the estimation of the values of the kinetic parameters were performed by fitting the experimental data of the components partial pressure to the kinetics equations. The goodness of fit was using statistical test including mean absolute relative residual. The mean absolute relative residual (MARR)

between experimental and calculated consumption rate of direct CO_2 hydrogenation (CDH) is defined as [43]:

$$\mathrm{MARR} = \sum_{i=1}^{N_{\exp}} \left| \frac{r_{\exp} - r_{\mathrm{cal}}}{r_{\exp}} \right| \times \frac{1}{N_{\exp}} \times 100 \tag{10}$$

Where $r_{\exp}$ is the experimental reaction rate, r_{cal} is model reaction rate and $N_{\exp}$ is the number of data points included. In addition, in fitting process, R^2 is a parameter for discrimination of results and it is compared calculated and experimental reaction rates and defined as [26]:

$$R^2 = 1 - (\text{residual sum of squares})/(\text{corrected sum of squares}) \tag{11}$$

The temperature dependence of the reaction rate constant is evaluated according to the Arrhenius-type equations:

$$k_{\mathrm{FT}} = k_{\mathrm{FT0}} \exp\left(\frac{-E_{\mathrm{a},i}}{RT}\right) \tag{12}$$

Where, E_{a} is activation energy for overall reaction rates that is determined from rate determination state (RDS) in considered models. Adsorption enthalpy ΔH_{ads}, can be determined via equilibrium constant for adsorption using the Van't Hoff equation:

$$K_i = K_{i0} \exp\left(\frac{-\Delta H_{\mathrm{ad},i}}{RT}\right) \tag{13}$$

Based on Eq. (13) the adsorption enthalpy $\Delta H_{\mathrm{ads},b}$ can be determined with adsorption parameter b via Eq. (14);

$$b = \frac{K_1}{K_3} = \frac{K_{1_0}}{K_{3_0}} \exp\left(\frac{-\Delta H_{\mathrm{ad},a}}{RT}\right) \tag{14}$$

Where, K_1 and K_3 are adsorption constants for surface adsorptions of CO and H_2O molecules, respectively. Thus, the apparent heat of adsorption for the combined term b is equal to following equation:

$$|\Delta H_{\mathrm{ads},b}| = \Delta H_{\mathrm{ads,CO}} - \Delta H_{\mathrm{ads,H_2O}} \tag{15}$$

3. Experimental

3.1. Catalyst preparation

The iron catalysts promoted with copper and potassium were prepared via precipitation technique. A solution containing $Fe(NO_3)_3$ (99.9+%; Fluka Chemical Co), $Cu(NO_3)_2$ (99.9+%; Fluka Chemical Co.), with an Fe/Cu mol ratio of 43.7 was introduced into a precipitation vessel containing deionized water and tert-butanol (t-BuOH, from Riedel-de Haën Co., 99.5%) solution at 350 K. A NH_4OH solution (Fluka Chemical Co.) was added simultaneously into this precipitation vessel to maintain the pH at a constant value of 7.0 ± 0.1, as measured with a pH meter. After precipitation, the precipitate was washed with deionized water, filtered and impregnated with potassium solution. A K_2CO_3 (99.9+%, Fluka Chemical Co.) solution in the amounts required to obtain the desired K/Fe weight ratio of 3/100 were added to the filter cake, and the mixture was then reslurried. The obtained catalyst precursors were dried over night at 393 K and calcined at 773 K for 5 h. The final obtained catalysts were composed of 100 Fe/3 K/2.6 Cu (Fe/Cu/K) in mass ratio, respectively.

In order to achieve a series of samples with different particle sizes, the surface tension for solvent in precipitation step varied from 55.8 to 15.9 (mN/m) by increasing the alcohol content of the solvent from 20 to 80 (vol%). The details of preparation procedure were reported in our previous work [44].

3.2. Characterization of catalysts

The catalysts particle sizes are determined by X-ray diffraction (XRD), transmission electron microscope (TEM) and Brunauer, Emmett and Teller (BET) techniques. The XRD spectrum of the samples was collected using an X-ray diffractometer, Philips PW1840 X-ray diffractometer, using monochromatized Cu/K_α radiation (40 kV, 40 mA) and a step scan mode at a scan rate of 0.02° (2θ) per second from 10°–80°. The average crystallite size of samples, d_{XRD}, can be estimated from XRD patterns by applying the Scherrer equation [17,45,46].

The total surface areas and average pore size of the fresh iron-based catalysts were estimated by the Brunauer, Emmett and Teller (BET) approach and Barrett–Joyner–Halenda (BJH) method using a Micromeritics ASAP 2010 equipment. The samples (ca. 200 mg) were degassed at 473 K for 24 h prior to analysis.

The morphology of prepared iron nanoparticles after calcinations was observed with a transmission electron microscope (TEM, LEO 912 AB, Germany). The average particle size (d_{TEM}) was obtained from TEM images by considering more than 100 particles and listed in Table 5.

3.3. Experimental apparatus and procedure

CO_2 hydrogenation reaction rates were measured in a continuous spinning basket reactor with electrical temperature controllers and mechanical backpressure valve for reaction pressure controlling. A detailed description of the experimental setup and procedures has been provided in our previous work [20,33,47,48]. About 3 g of the fresh iron catalysts (catalyst particle size varied from 38 to 14 nm) diluted with 30 cm^3 inert silica sand loaded to the reactor. It has been found that iron carbides (Fe_xC_y) are the active phase in FTS the reaction [6]. Thus, the iron catalysts were activated with two-step protocol for transformation of hematite to iron carbides ($Fe_2O_3 \rightarrow Fe_3O_4 \rightarrow Fe_xC_y$) during the pre-treatment in situ the reactor. In the first step, the catalysts were reduced by a 5% (v/v) of H_2/N_2 gas mixture with space velocity of 15.1 NL/g_{cat}/h at atmospheric pressure and 1800 rpm. Thermodynamics predicts under which conditions a catalyst can be reduced. The reduction of metal oxides to metals will proceed when the change in Gibbs free energy, ΔG, has a negative value. The Gibbs free energy for reduction process is related to Gibbs free energy for the reduction under standard conditions (ΔG^0) and partial pressures of hydrogen and water. For many oxides, such as those of cobalt, nickel and the noble metals, the ΔG^0 is already negative and reduction is thermodynamically feasible. But the iron oxide have a positive ΔG^0 and for an effective reduction, the partial pressure of hydrogen must be decreased by dilution of hydrogen [49]. In our reduction process, the hydrogen is diluted by nitrogen. The temperature of reactor increased to 673 K with a heating rate of 5 K/min, maintained for 1 h at this temperature, and then reduced to 543 K. In the second step of activation procedure, the iron oxides were changed to carbide form by the synthesis gas stream with H_2/CO molar ratio equal to 1 and space velocity of 3.07 NL/g_{cat}/h for 24 h at atmospheric pressure and 543 K. After catalyst reduction and activation, the carbon dioxide and hydrogen gases were fed to the reactor and reaction operation change to 563 K, 17 bar, H_2/CO_2 molar ration equal to 3 and a space velocity of 4.9 NL/g_{cat}/h. After reaching steady state, the kinetic of the CO_2 hydrogenation reaction rate was measured.

During kinetics measurement runs, three levels of temperatures (543, 563 and 583 K) were evaluated. In addition, the space velocity of the synthesis gas varied between 2.4 and 8.4 NL/g_{cat}/h. The total pressure of the reaction, H_2/CO_2 molar ratio in the feed and stirring speed of the reactor basket were fixed at 17 bar, 3 and 1800 rpm, respectively [48]. Conversion of carbon dioxide and hydrogen, and the formation of various products were measured with

Table 1. Experimental operation conditions and rate of CO_2 hydrogenation (r_{CDH}) for catalyst with 38 nm particle size.

Run no.	Temperature (K)	GHSV (NL/g_{cat}/h)	Pressure (bar)				r_{CDH} (mol/g_{cat}/h)	
			P_{CO_2}	P_{H_2O}	P_{CO}	P_{H_2}	Experimental	Model
1	543	2.4	3.33	2.02	0.25	10.52	0.0053	0.0053
2		3.5	3.53	1.59	0.21	10.99	0.0061	0.0061
3		4.9	3.68	1.26	0.17	11.35	0.0068	0.0067
4		6.5	3.79	1.00	0.14	11.64	0.0071	0.0071
5		8.4	3.89	0.79	0.11	11.87	0.0073	0.0074
6	563	2.4	3.13	2.42	0.32	10.07	0.0062	0.0063
7		3.5	3.37	1.91	0.26	10.64	0.0072	0.0072
8		4.9	3.55	1.51	0.22	11.08	0.0080	0.0079
9		6.5	3.70	1.19	0.18	11.43	0.0084	0.0084
10		8.4	3.81	0.94	0.14	11.70	0.0086	0.0087
11	583	2.4	2.89	2.92	0.41	9.53	0.0074	0.0074
12		3.5	3.18	2.29	0.33	10.21	0.0085	0.0085
13		4.9	3.40	1.81	0.27	10.75	0.0094	0.0093
14		6.5	3.58	1.43	0.22	11.17	0.0099	0.0099
15		8.4	3.72	1.13	0.18	11.50	0.0101	0.0103

Table 2. Experimental operation conditions and rate of CO_2 hydrogenation (r_{CDH}) for catalyst with 28 nm particle size.

Run no.	Temperature (K)	GHSV (NL/g_{cat}/h)	Pressure (bar)				r_{CDH} (mol/g_{cat}/h)	
			P_{CO_2}	P_{H_2O}	P_{CO}	P_{H_2}	Experimental	Model
1	543	2.4	3.27	2.13	0.29	10.39	0.0055	0.0055
2		3.5	3.44	1.75	0.24	10.82	0.0066	0.0067
3		4.9	3.58	1.43	0.20	11.16	0.0076	0.0076
4		6.5	3.70	1.18	0.17	11.45	0.0083	0.0083
5		8.4	3.79	0.97	0.15	11.68	0.0089	0.0089
6	563	2.4	3.06	2.57	0.36	9.91	0.0065	0.0065
7		3.5	3.27	2.10	0.31	10.43	0.0078	0.0079
8		4.9	3.44	1.72	0.26	10.85	0.0090	0.0090
9		6.5	3.58	1.41	0.22	11.19	0.0098	0.0098
10		8.4	3.70	1.16	0.18	11.47	0.0105	0.0105
11	583	2.4	2.79	3.09	0.46	9.34	0.0077	0.0077
12		3.5	3.05	2.52	0.39	9.97	0.0092	0.0093
13		4.9	3.27	2.06	0.33	10.48	0.0106	0.0106
14		6.5	3.44	1.69	0.28	10.89	0.0116	0.0116
15		8.4	3.58	1.39	0.23	11.22	0.0123	0.0123

Table 3. Experimental operation conditions and rate of CO_2 hydrogenation (r_{CDH}) for catalyst with 21 nm particle size.

Run no.	Temperature (K)	GHSV (NL/g_{cat}/h)	Pressure (bar)				r_{CDH} (mol/g_{cat}/h)	
			P_{CO_2}	P_{H_2O}	P_{CO}	P_{H_2}	Experimental	Model
1	543	2.4	3.22	2.24	0.31	10.27	0.0058	0.0057
2		3.5	3.38	1.88	0.27	10.66	0.0071	0.0071
3		4.9	3.52	1.58	0.24	11.00	0.0083	0.0083
4		6.5	3.63	1.33	0.21	11.27	0.0092	0.0092
5		8.4	3.73	1.12	0.18	11.50	0.0100	0.0100
6	563	2.4	2.99	2.70	0.40	9.77	0.0068	0.0068
7		3.5	3.19	2.26	0.34	10.25	0.0083	0.0084
8		4.9	3.36	1.89	0.30	10.65	0.0098	0.0098
9		6.5	3.50	1.59	0.26	10.98	0.0109	0.0109
10		8.4	3.62	1.34	0.23	11.26	0.0118	0.0118
11	583	2.4	2.71	3.25	0.50	9.16	0.0080	0.0080
12		3.5	2.96	2.72	0.44	9.75	0.0098	0.0099
13		4.9	3.17	2.27	0.38	10.23	0.0115	0.0115
14		6.5	3.34	1.91	0.33	10.63	0.0128	0.0128
15		8.4	3.48	1.60	0.29	10.97	0.0138	0.0138

a period of 12 h at each new condition. Periodically during the run, the catalyst activity was measured at preset "standard" condition (a space velocity equal to 4.9 NL/g_{cat}/h) to check the catalyst deactivation.

In the experimental setup a cold trap is considered for collection of produced higher hydrocarbons and water [36]. After each kinetic run, the produced water and hydrocarbons were separated and each product was weighted carefully. The water partial pressure was determined by collecting the produced water in the trap, separating it from the oil, and determining its amount by weighing. The weight of water has been converted to partial pressure in the reactor based upon the ideal gas law. The partial pressures of CO, CO_2, H_2O and H_2 and hydrocarbon production rate (r_{CDH}) experimental and model are listed in Tables 1–4.

The products were analyzed by a combination of two gas chromatographs (Varian CP-3800) equipped with TCD and FID detectors. A packed column contains molecular sieve13x and Hayesep Q CP1069, which is connected to TCD detector, and a capillary column (CP fused silica with 25 m × 0.25 mm × 0.2 μm film thickness) connected to FID detector [20,47,48]. Hydrogen was analyzed through Shimadzu, GC PTF 4C, equipped with TCD detector and two columns in series (Propack-Q with 2 m length, and

Table 4. Experimental operation conditions and rate of CO_2 hydrogenation (r_{CDH}) for catalyst with 14 nm particle size.

Run no.	Temperature (K)	GHSV (NL/g_{cat}/h)	Pressure (bar)				r_{CDH} (mol/g_{cat}/h)	
			P_{CO_2}	P_{H_2O}	P_{CO}	P_{H_2}	Experimental	Model
1	543	2.4	3.15	2.37	0.34	10.12	0.0060	0.0061
2		3.5	3.30	2.05	0.29	10.48	0.0077	0.0077
3		4.9	3.43	1.78	0.24	10.78	0.0095	0.0094
4		6.5	3.54	1.54	0.20	11.04	0.0110	0.0110
5		8.4	3.63	1.34	0.17	11.27	0.0125	0.0125
6	563	2.4	2.91	2.85	0.44	9.59	0.0071	0.0071
7		3.5	3.09	2.47	0.37	10.02	0.0091	0.0091
8		4.9	3.25	2.13	0.31	10.39	0.0111	0.0111
9		6.5	3.38	1.85	0.26	10.71	0.0130	0.0130
10		8.4	3.50	1.60	0.22	10.98	0.0147	0.0146
11	583	2.4	2.61	3.43	0.57	8.96	0.0083	0.0083
12		3.5	2.84	2.96	0.48	9.48	0.0106	0.0108
13		4.9	3.03	2.56	0.40	9.93	0.0131	0.0131
14		6.5	3.20	2.22	0.34	10.31	0.0152	0.0152
15		8.4	3.34	1.92	0.29	10.64	0.0172	0.0170

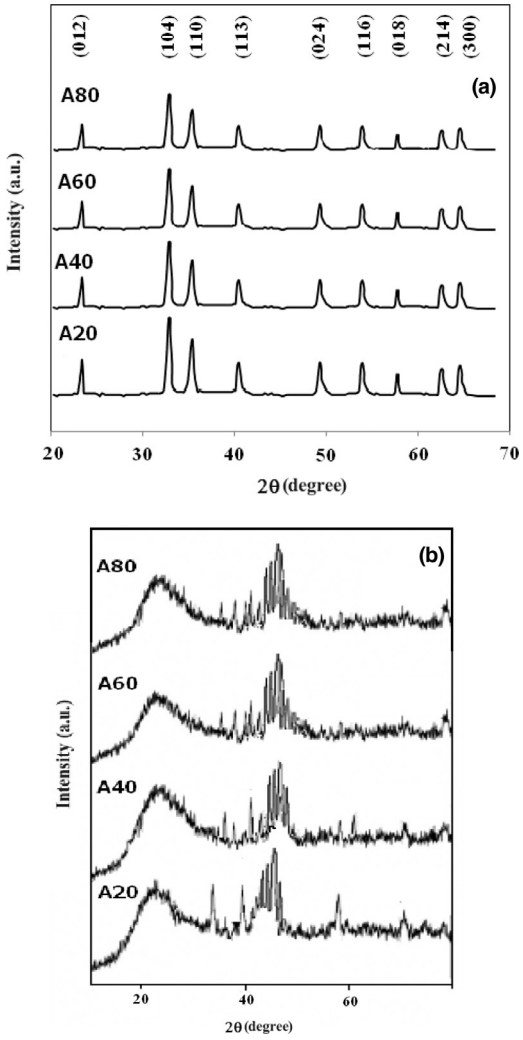

Fig. 1. XRD patterns of iron catalysts prepared in alcohol/water system with alcohol percentage after calcinations (a) and after reaction (b): (A20) 20 alcohol vol%, (A40) 40 alcohol vol%, (A60) 60 alcohol vol%, and (A80) 80 alcohol vol%.

3 mm OD for CO_2, C_2H_4 and C_2H_6 separation and molecular sieve-5A with 2 m length, and 3 mm OD for CO, N_2, CH_4 and O_2 separation), which were connected to each other via a three-way valve.

4. Results and discussion

4.1. Catalysts characterization

The XRD patterns of the prepared catalysts after calcination and reaction are shown in Fig. 1(a) and (b). All the diffraction peaks in Fig. 1(a) (fresh catalysts) can be indexed to the rhombohedra phase of α-Fe_2O_3 nanoparticles with space group R-3C (167), which is in good agreement with the literature value (JCPDS Card No. 33-0664) [50,51].

As show in Fig. 1, by decreasing the alcohol content in precipitation system, the peak heights and as a results the FWHMs (full width at half maximum) of the XRD patterns are decreased, which are related to decreasing of crystallite size. The strong and sharp peaks suggested that Fe_2O_3 crystals are highly crystalline. However, the broadening in the reflection peaks was due to the particles size at nano domain, which increased by decreasing of catalyst nano particle size for alcohol content in the solvent from 20 to 80 (vol%). It was also shown in Fig. 1 that the presence of lanthanum and copper promoters and the alcohol content in the solvent do not affect the hematite crystalline phases, showing that the water/alcohol ratio do not change the precipitation mechanism. The characteristic peak at $2\theta = 33.3°$ which corresponds to the hematite 104 plane was used to calculate the average metal particle size by the Scherrer equation [52]. The calculated values of d_{XRD} of the samples are listed in Table 5.

As shown in Fig. 1(b) (used catalysts) a series of diffraction peaks are observed under pretreatment at ca. 39°–44°, in the XRD profiles irrespective of the iron carbide phases. Before the XRD measurements, the used catalysts were passivated in 1% O_2/He stream at room temperature inside the reactor. According to the JCPDS card, the $\acute{\varepsilon}$-$Fe_{2.2}C$ carbide shows a main diffraction peak near 43° and the peaks at ca. 39° and 41° are used for identification of Hägg carbide (χ-$Fe_{2.5}C$) (JCPDS 36-1248) [53]. Peak assignation was based on the characteristic angles of cementite carbide (θ-Fe_3C) (JCPDS 76-1877) at 78.0° and 70.1°, which are not presented in the diffractogram of the sample χ-$Fe_{2.5}C$ [16]. In addition, the peaks that are observed at 35°, 57° and 63° were assigned to Fe_3O_4. As shown in Fig. 1(b), the catalysts with higher alcohol in preparation process, have higher amount of the cementite carbides (θ-Fe_3C) and magnetite (Fe_3O_4). These results may be related to higher activity of the catalysts in CO_2 hydrogenation that increased the concentration of oxidizing products (H_2O) in reaction atmosphere. The produced H_2O converted the $\acute{\varepsilon}$-$Fe_{2.2}C$ carbides into the Hägg carbide (χ-$Fe_{2.5}C$) and subsequently into the cementite (θ-Fe_3C) with lower carbon content and magnetite (Fe_3O_4) [4].

Table 5. Water/alcohol ratio, surface tension of solvent, BET surface are and average particle size determined by TEM, BET and XRD techniques.

Solvent	Alcohol (vol%)	Surface tension[a] (mN/m)	Average pore size[b] (nm)	Surface area (m^2/g)	Particle size (nm)	
					d_{TEM}	d_{XRD}
t-BuOH/water	20	55.8	38.9	32	38	33
	40	42.1	24.9	44	28	26
	60	29.2	20.8	60	21	20
	80	15.9	13.1	95	14	15

[a] Temperature = 298 K.
[b] These values were calculated by BJH method from desorption isotherm.

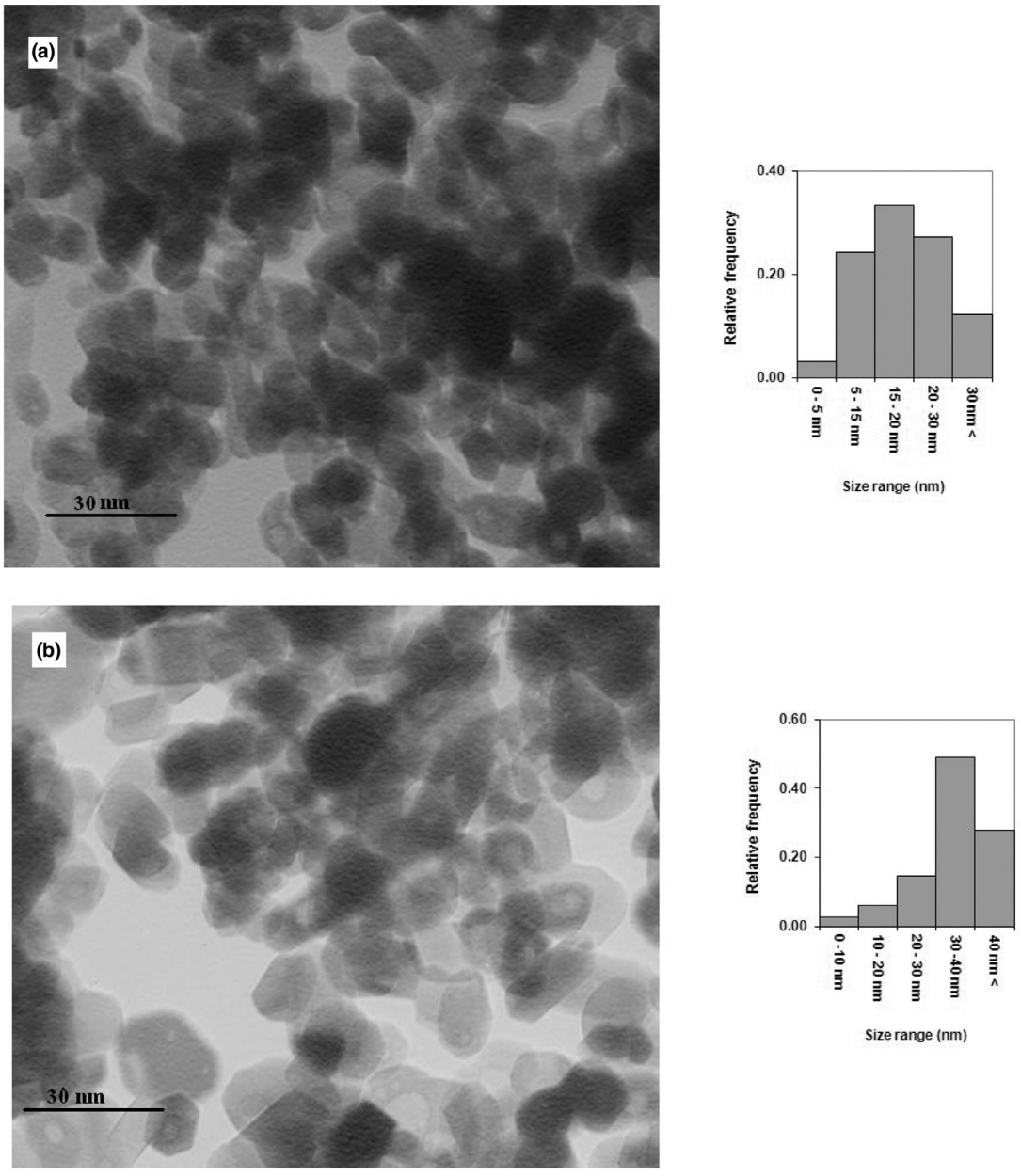

Fig. 2. TEM images of Fe_2O_3 nanoparticles prepared in t-BuOH/water system with alcohol percentage after calcination: (a) 60 alcohol vol%, (b) 20 alcohol vol%.

BET surface areas and average pore sizes of the prepared iron catalysts after calcination are shown in Table 5. However, the average pore sizes of the catalysts were calculated by Barett–Joyner–Halenda (BJH) method. As shown in this table, surface areas and particle sizes of the prepared iron catalysts were changed with surface tension of precipitated solvent. As shown in Table 5, the dimension of the prepared hematite nanoparticles depended directly on the surface tension of the solvent and decreased with decreasing of solvent surface tension. The surface tension is affected on supersaturation condition in precipitation process [44,54,55].

The TEM photographs for the prepared samples are demonstrated in Fig. 2 and calculated nanoparticle dimensions were listed in Table 5. As shown in Fig. 2 and Table 5, the average range of particle size decreased for alcohol content in the solvent from 20 to

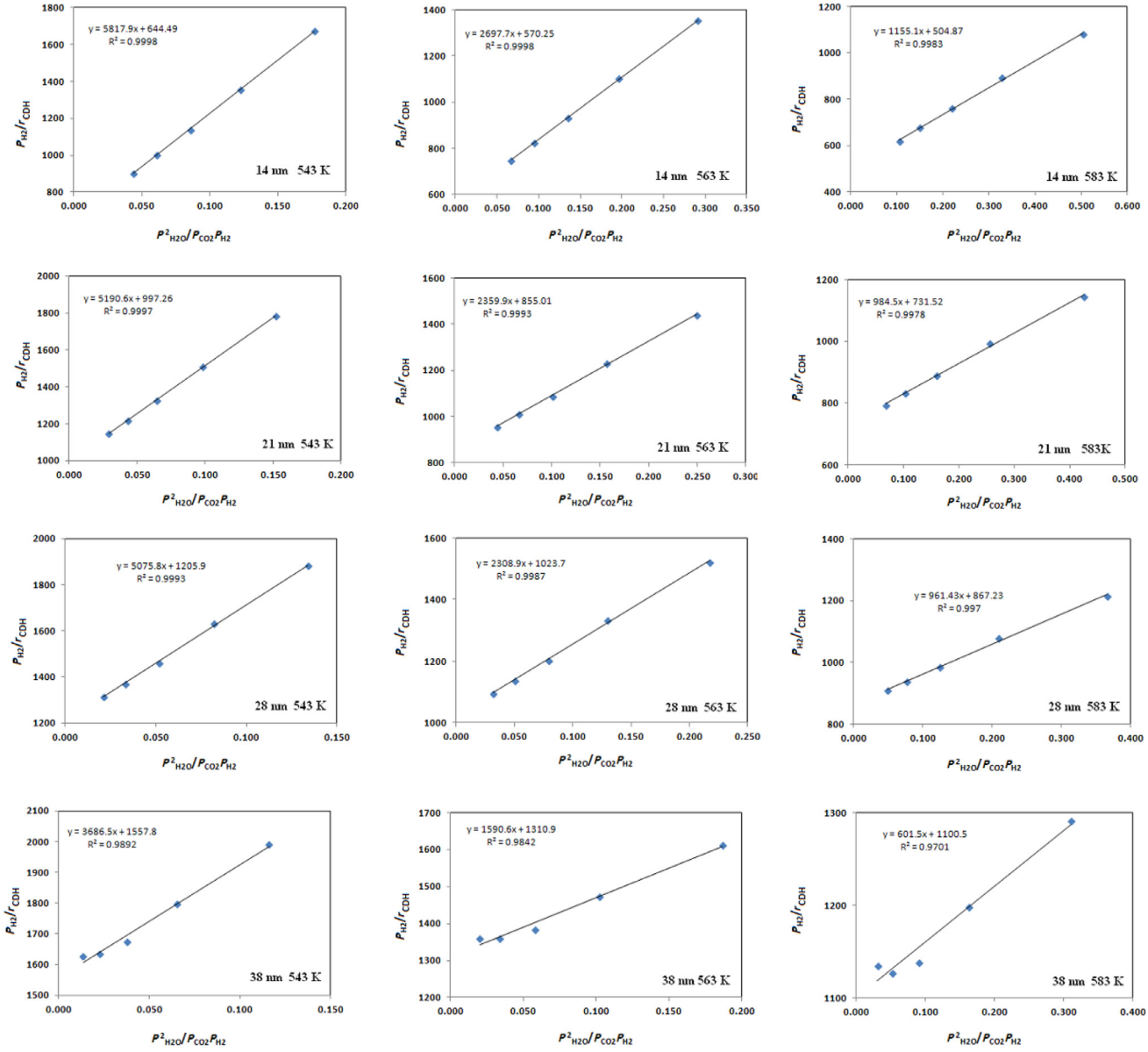

Fig. 3. Linearised plot of $\frac{P_{H_2}}{r_{CDH}}$ versus $\frac{P^2_{H_2O}}{P_{CO_2}P_{H_2}}$ for the prepared catalysts.

80 (vol%). As shown in Table 5, the experimental results for catalyst particle sizes obtained from different techniques are comparable with each other. This shows that no accumulations are present in prepared nanoparticles. However, the TEM results are considered as references for kinetic consideration.

4.2. Kinetic model parameters

Tables 1–4, lists the experimental and calculated results for CO_2 hydrogenation (CDH) to higher hydrocarbons. These results show that the reaction rates are increased by decreasing of catalyst particle size because of increased surface-to-volume ratios and chemical potentials in lower particle size [18,34,56–58]. In the heterogeneous catalysts, only surface of catalysts particles can interact with the other reactants; therefore, more particles are able to react, and the reaction rate increases.

Fig. 3 shows the linearized plot of $\frac{P_{H_2}}{r_{CDH}}$ versus $\frac{P^2_{H_2O}}{P_{CO_2}P_{H_2}}$ for the prepared iron catalysts with varied particle sizes. Table 6 listed the calculated kinetic parameters for prepared catalysts and MARR and R^2 results. As shown in Fig. 3 and listed in Tables 1–4 and 6, the parameter estimation obtained for the model provides a satisfactory fitting between experimental and model CO_2 hydrogenation results. As shown in Table 6, the MARR and R^2 results are varied for all iron catalysts from 0.33 to 0.98 and 0.96 to 0.99 respectively, and good agreement between the model and experience results can be seen. This means that Eq. (7) is a good model for kinetic evaluation of our prepared iron catalysts in our experimental conditions.

As shown in Table 6, the rate constants for direct CO_2 hydrogenation (k_{FTS}) are increased from 6.4×10^{-4} to 9.1×10^{-4}, 8.3×10^{-4} to 1.2×10^{-3}, 1.0×10^{-3} to 1.4×10^{-3} and 1.6×10^{-3} to 2.0×10^{-3} for catalysts with 38 nm, 28 nm, 21 nm and 14 nm particle size, respectively (by increasing of the reaction temperature from 543 K to 583 K). In addition, the adsorption parameters (b) are decreased from 1.6×10^{-2} to 1.0×10^{-2}, 3.8×10^{-2} to 2.8×10^{-2}, 5.9×10^{-2} to 4.4×10^{-2} and 1.2×10^{-1} to 9.5×10^{-2} for catalysts with 38 nm, 28 nm, 21 nm and 14 nm particle sizes, respectively. These results show that the rate constant (k_{FTS}) and the

Table 6. Final estimates for the parameters of the CO_2 hydrogenation kinetic models.

Catalyst particle size (nm)	Temperature (K)	Model parameters		E_{app} (kJ/mol)	ΔH_b (kJ/mol)	MARR	R^2
		k_{FTS} mol/(g_{cat} h bar)	b				
38	543	6.4×10^{-4}	1.6×10^{-2}	23	−28.5	0.98	0.96
	563	7.6×10^{-4}	1.3×10^{-2}				
	583	9.1×10^{-4}	1.0×10^{-2}				
28	543	8.3×10^{-4}	3.8×10^{-2}	21.7	−18.6	0.35	0.98
	563	9.8×10^{-4}	3.4×10^{-2}				
	583	1.2×10^{-3}	2.8×10^{-2}				
21	543	1.0×10^{-3}	5.9×10^{-2}	20.4	−18.1	0.33	0.99
	563	1.2×10^{-3}	5.2×10^{-2}				
	583	1.4×10^{-3}	4.4×10^{-2}				
14	543	1.6×10^{-3}	1.2×10^{-1}	16.1	−16.2	0.43	0.99
	563	1.8×10^{-3}	1.1×10^{-1}				
	583	2.0×10^{-3}	9.5×10^{-2}				

adsorption parameter (b) for CO_2 hydrogenation are decreased by increasing of the catalysts particle size. These results suggest that reducing the catalyst particle size increase both the amount of adsorption of the reactants and catalytic activity of reaction, simultaneity. Smaller nanoparticles have higher surface energies and thus should be more prone to surface reconstruction, which can lead to different catalytic dynamics for different sized nanoparticles [56,58,59].

As shown in Table 6, the values of activation energies for direct CO_2 hydrogenation reaction are fall within the narrow range of 23–16 kJ/mol [14]. It is important to notice that these values of the FTS activation energies are lower than those reported in the technical literatures (between 75 and 110 kJ/mol) [22,37,60]. As reported in previous section, the direct CO_2 hydrogenation to higher hydrocarbons (CDH) by iron catalysts is performed in two-steps. In the first step, the CO_2 is reduced to carbon monoxide and water according to the reverse water gas shift reaction (Eq. (1)). In the second step, produced carbon monoxide can then further react with hydrogen, according to the overall FTS reaction, which is producing higher hydrocarbons. Thus, the FTS reaction is limited by CO generation in the first step and produced activated carbon monoxide on the surface of the catalyst may be converted to higher hydrocarbons via FTS reaction. The occurrence of the RWGS reaction before FTS reaction, which produced the activated surface CO species, is reduced the activation energy of the FTS reaction.

Table 6 compares the adsorption parameter (b) for catalysts with different particle sizes. As listed in Table 7, with decreasing the catalyst particle size from 38 nm to 14 nm, the adsorption parameter (b) and adsorption enthalpy ($\Delta H_{ads,b}$) are increased. As shown in Eq. (15), increasing of the adsorption enthalpy ($\Delta H_{ads,b}$) can be due to an increasing in the adsorption equilibrium constant for water and/or an decreasing in the adsorption equilibrium constant for carbon monoxide. These results may be related to RWGS reaction as an introduction of FTS reaction in CO_2 hydrogenation to higher hydrocarbons process.

5. Conclusions

Experiments for the kinetics evaluation of the indirect CO_2 hydrogenation reaction are carried out over a series precipitated copper and potassium promoted iron catalysts in a well mixed, continuous spinning basket reactor over a wide range of industrially relevant reaction conditions. For evaluation of structure sensitivity of indirect CO_2 hydrogenation to higher hydrocarbons, the kinetics parameters of developed model are evaluated for a series of iron catalysts with various particle sizes. In order to achieve a series of samples with different particle sizes, the surface tension for solvent in precipitation step varied from 55.8 to 15.9 (mN/m) by increasing the alcohol content of the solvent from 20 to 80 (vol%). The precipitation process was done in various alcohol/water mixtures to achieve a series of catalyst particle sizes between 38 and 14 nm.

A new kinetic model was developed for two-steps direct CO_2 hydrogenation to higher hydrocarbons via RWGS and FTS mechanisms. In the first step, the CO_2 is reduced to carbon monoxide and water according to the RWGS reaction. In the second step, produced carbon monoxide can then further react with hydrogen, according to the overall FTS reaction, which is producing higher hydrocarbons. Thus, the FTS reaction is limited by CO generation in the first step and produced activated carbon monoxide on the surface of the catalyst may be converted to higher hydrocarbons via FTS reaction. The occurrence of the RWGS reaction before FTS reaction, which is produced the activated surface CO species, is reduced the activation energy of the FTS reaction and RWGS reaction as an introduction of FTS reaction in CO_2 hydrogenation to higher hydrocarbons process.

Acknowledgments

Financial support of the Ferdowsi University of Mashhad, Iran (2/38699-21/7/94) is gratefully acknowledged.

References

[1] B. Hu, C. Guild, S.L. Suib, J. CO_2 Util. 1 (2013) 18–27.
[2] R.W. Dorner, D.R. Hardy, F.W. Williams, H.D. Willauer, Catal. Commun. 15 (2011) 88–92.
[3] S. Saeidi, N.A.S. Amin, M.R. Rahimpour, J. CO_2 Util. 5 (2014) 66–81.
[4] T. Herranz, S. Rojas, F.J. Pérez-Alonso, M. Ojeda, P. Terreros, J.L.G. Fierro, Appl. Catal. A 311 (2006) 66–75.
[5] C. Hao, S. Wang, M. Li, L. Kang, X. Ma, Catal. Today 160 (2011) 184–190.
[6] G.P. Van Der Laan, A.A.C.M. Beenackers, Catal. Rev. 41 (1999) 255–318.
[7] A. Nakhaei Pour, M.R. Housaindokht, S.F. Tayyari, J. Zarkesh, J. Nat. Gas Chem. 19 (2010) 107–116.
[8] A. Nakhaei Pour, M. Housaindokht, Catal. Lett. 143 (2013) 1328–1338.
[9] I. Dimitriou, P. Garcia-Gutierrez, R.H. Elder, R.M. Cuellar-Franca, A. Azapagic, R.W.K. Allen, Energy Environ. Sci. 8 (2015) 1775–1789.
[10] U. Burghaus, New and Future Developments in Catalysis, Elsevier, Amsterdam, 2013, pp. 27–47.
[11] M. Aresta, Carbon Dioxide as Chemical Feedstock, John Wiley & Sons, 2010.
[12] O.R. Inderwildi, S.J. Jenkins, D.A. King, J. Phys. Chem. C 112 (2008) 1305–1307.
[13] K.M.K. Yu, I. Curcic, J. Gabriel, S.C.E. Tsang, Chem.Sus.Chem. 1 (2008) 893–899.
[14] T. Riedel, G. Schaub, K.-W. Jun, K.-W. Lee, Ind. Eng. Chem. Res. 40 (2001) 1355–1363.
[15] M. Iglesias, R. Edzang, G. Schaub, Catal. Today 215 (2013) 194–200.
[16] A. Nakhaei Pour, M.R. Housaindokht, J. Zarkesh, S.F. Tayyari, J. Ind. Eng. Chem. 16 (2010) 1025–1032.
[17] A. Nakhaei Pour, M.R. Housaindokht, J. Nat. Gas Sci. Eng. 14 (2013) 29–33.
[18] A. Nakhaei Pour, M.R. Housaindokht, J. Ind. Eng. Chem. 20 (2014) 591–596.
[19] M.E. Dry, Studies in Surface Science and Catalysis, Elsevier, 2004, pp. 533–600.
[20] A. Nakhaei Pour, H. Khodabandeh, M. Izadyar, M. Housaindokht, React. Kinet. Mech. Catal. 111 (2014) 29–44.
[21] A. Nakhaei Pour, Z. Keyvanloo, M. Izadyar, S.M. Modaresi, Int. J. Hydrog. Energy 40 (2015) 7064–7071.
[22] G.P. Van Der Laan, A. Beenackers, Catal. Rev. Sci. Eng. 41 (1999) 255–318.
[23] B. Deng, X. Pang, Chin. Sci. Bull. 52 (2007) 3179–3182.
[24] S.-H. Kwack, M.-J. Park, J. Bae, K.-S. Ha, K.-W. Jun, React. Kinet. Mech. Catal. 104 (2011) 483–502.

[25] R. Ohata, N. Tomita, Y. Ikada, J. Colloid Interface Sci. 270 (2004) 413–416.
[26] B.-T. Teng, J. Chang, J. Yang, G. Wang, C.-H. Zhang, Y.-Y. Xu, H.-W. Xiang, Y.-W. Li, Fuel 84 (2005) 917–926.
[27] N. Fischer, R. Henkel, B. Hettel, M. Iglesias, G. Schaub, M. Claeys, Catal. Lett. 146 (2016) 509–517.
[28] R.E. Owen, P. Plucinski, D. Mattia, L. Torrente-Murciano, V.P. Ting, M.D. Jones, J. CO_2 Util. 16 (2016) 97–103.
[29] X. Wang, G. Yang, J. Zhang, S. Chen, Y. Wu, Q. Zhang, J. Wang, Y. Han, Y. Tan, Chem. Commun. 52 (2016) 7352–7355.
[30] H.D. Willauer, R. Ananth, M.T. Olsen, D.M. Drab, D.R. Hardy, F.W. Williams, J. CO_2 Util. 3–4 (2013) 56–64.
[31] G.L. Bezemer, J.H. Bitter, H.P.C.E. Kuipers, H. Oosterbeek, J.E. Holewijn, X. Xu, F. Kapteijn, A.J. van Dillen, K.P. de Jong, J. Am. Chem. Soc. 128 (2006) 3956–3964.
[32] G.L. Bezemer, A. van Laak, A.J. van Dillen, K.P. de Jong, Studies in Surface Science and Catalysis, Elsevier, 2004, pp. 259–264.
[33] A. Nakhaei Pour, M.R. Housaindokht, M. Irani, S.M. Kamali Shahri, Fuel 116 (2014) 787–793.
[34] R.A. van Santen, M.M. Ghouri, S. Shetty, E.M.H. Hensen, Catal. Sci. Technol. 1 (2011) 891–911.
[35] W. Ma, G. Jacobs, D.E. Sparks, M.K. Gnanamani, V.R.R. Pendyala, C.H. Yen, J.L. Klettlinger, T.M. Tomsik, B.H. Davis, Fuel 90 (2011) 756–765.
[36] A. Nakhaei Pour, M.R. Housaindokht, J. Zarkesh, M. Irani, E.G. Babakhani, J. Ind. Eng. Chem. 18 (2012) 597–603.
[37] G.P. van der Laan, A.A.C.M. Beenackers, Appl. Catal. A 193 (2000) 39–53.
[38] S. Krishnamoorthy, A. Li, E. Iglesia, Catal. Lett. 80 (2002) 77–86.
[39] A.Nakhaei Pour, S.M.K. Shahri, Y. Zamani, A. Zamanian, J. Nat. Gas Chem. 19 (2010) 193–197.
[40] A. Nakhaei Pour, M. Housaindokht, F. Torabi, J. Iran. Chem. Soc. 11 (2014) 1639–1648.
[41] A. Nakhaei Pour, M.R. Housaindokht, J. Zarkesh, S.F. Tayyari, J. Nat. Gas Sci. Eng. 2 (2010) 79–85.
[42] A. Nakhaei Pour, M.R. Housaindokht, S.F. Tayyari, J. Zarkesh, S.M.K. Shahri, Chem. Eng. Res. Des. 89 (2011) 262–269.
[43] L. Nowicki, S. Ledakowicz, D.B. Bukur, Chem. Eng. Sci. 56 (2001) 1175–1180.
[44] A. Nakhaei Pour, M. Housaindokht, H. Monhemi, Colloid J. 76 (2014) 782–787.
[45] A. Nakhaei Pour, M.R. Housaindokht, J. Nat. Gas Sci. Eng. 14 (2013) 49–54.
[46] A. Nakhaei Pour, M.R. Housaindokht, J. Nat. Gas Sci. Eng. 14 (2013) 204–210.
[47] A. Nakhaei Pour, F. Riyahi, M.R. Housaindokht, M. Irani, S.M.K. Shahri, B. Hatami, J. Energy Chem. 22 (2013) 119–129.
[48] A. Nakhaei Pour, M.R. Housaindokht, J. Zarkesh, M. Irani, E.G. Babakhani, J. Ind. Eng. Chem. 18 (2012) 597–603.
[49] L. Holysz, A. Szczes, E. Chibowski, J. Colloid Interface Sci. 316 (2007) 996–1002.
[50] J. Nakagawa, N. Hirota, K. Kitazawa, M. Shoda, J. Appl. Phys. 86 (1999) 2923–2925.
[51] Y.-Z. Guo, D.-C. Yin, H.-L. Cao, J.-Y. Shi, C.-Y. Zhang, Y.-M. Liu, H.-H. Huang, Y. Liu, Y. Wang, W.-H. Guo, Int. J. Mol. Sci. 13 (2012) 16916–16928.
[52] P. Pourghahramani, E. Forssberg, Int. J. Miner. Process. 79 (2006) 106–119.
[53] J. Xu, C.H. Bartholomew, J. Phys. Chem. B 109 (2005) 2392–2403.
[54] M.R. Housaindokht, A. Nakhaei Pour, Solid-State Sci. 14 (2012) 622–625.
[55] H.-I. Chen, H.-Y. Chang, Colloids Surf. A Physicochem. Eng. Asp. 242 (2004) 61–69.
[56] D.Y. Murzin, J. Mol. Catal. A Chem. 315 (2010) 226–230.
[57] A.T. Bell, Science 299 (2003) 1688–1691.
[58] D.Y. Murzin, J. Catal. 276 (2010) 85–91.
[59] D.Y. Murzin, Chem. Eng. Sci. 64 (2009) 1046–1052.
[60] A. Nakhaei Pour, E. Hosaini, A. Tavasoli, A. Behroozsarand, F. Dolati, J. Nat. Gas Sci. Eng. 21 (2014) 772–778.